COMPAct: Computational Optimization and Automated Modular design of Planetary Actuators

Aman Singh*, Deepak Kapa*, Suryank Joshi, and Shishir Kolathaya

Abstract— The optimal design of robotic actuators is a critical area of research, yet limited attention has been given to optimizing gearbox parameters and automating actuator CAD. This paper introduces COMPAct: *Computational Optimization and Automated Modular Design of Planetary Actuators*, a framework that systematically identifies optimal gearbox parameters for a given motor across four gearbox types, single-stage planetary gearbox (SSPG), compound planetary gearbox (CPG), Wolfrom planetary gearbox (WPG), and double-stage planetary gearbox (DSPG). The framework minimizes mass and actuator width while maximizing efficiency, and further automates actuator CAD generation to enable direct 3D printing without manual redesign. Using this framework, optimal gearbox designs are explored over a wide range of gear ratios, providing insights into the suitability of different gearbox types across various gear ratio ranges. In addition, the framework is used to generate CAD models of all four gearbox types with varying gear ratios and motors. Two actuator types are fabricated and experimentally evaluated through power efficiency, no-load backlash, and transmission stiffness tests. Experimental results indicate that the SSPG actuator achieves a mechanical efficiency of 60–80%, a no-load backlash of $0.59°$, and a transmission stiffness of 242.7 Nm/rad, while the CPG actuator demonstrates 60% efficiency, $2.6°$ backlash, and a stiffness of 201.6 Nm/rad. Code available at: `https://anonymous.4open.science/r/COMPAct-SubNum-3408` Video: `https://youtu.be/99zOKgxsDho`

Fig. 1: COMPAct: Framework for optimal design and automated CAD generation of planetary robotic actuators.

I. INTRODUCTION

Computational robot design for optimal performance has attracted significant attention, particularly through design frameworks that optimize mechanical design for particular application. Studies such as [1]–[4] optimize link lengths, transmission ratios, and spring stiffness but exclude gearboxes. Similarly, [5] considers link lengths and actuator attachments without optimizing gearbox parameters. Other efforts [6], [7] apply design optimization to manipulators and monopeds, including gear ratios, compliance, and mass, yet without addressing gearbox type, efficiency, or weight. Additional works [8]–[10] incorporate motor and gearbox friction but focus on belt drives rather than planetary gears. Most approaches thus overlook gearbox design or treat ratios without considering efficiency, mass, or gearbox type, often using simplified mass models.

There are a few exceptions that focus on gearbox optimization, like [11], [12] focus on compound and single-stage planetary gearboxes by optimizing tooth counts and module but ignore mass and efficiency. Likewise, [13] studies a Wolfrom (3K) gearbox, reducing mass by minimizing tooth counts instead of using detailed models, and without addressing efficiency.
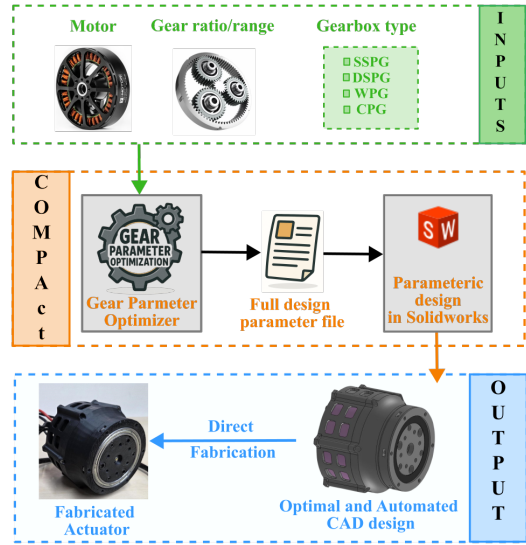
Beyond optimization, considerable research has also focused on automating CAD design. Large language models (LLMs) have been explored for CAD automation [14], [15], but remain at an early stage and cannot yet handle complex systems such as actuators or gearboxes. A more reliable approach is parametric CAD design [16], [17], where geometric dimensions are defined as variables and updates propagate automatically. Examples include parametric turbomachinery blades [18] and an automated framework for helical gearboxes [19]. To our knowledge, no prior work has automated the CAD design of planetary gearboxes for robotic actuators.

There has been a growing interest in 3D-printed actuators for robotic joints. While CNC-machined actuators deliver higher performance, 3D-printed ones enable rapid prototyping, lower cost, and faster iteration. Prior work has demonstrated their promise in planetary actuators [20], [21], wearable exoskeletons [22], humanoid and quadrupedal platforms [23], [24], and hobbyist projects [25], [26]. However, these designs are restricted to fixed gear ratios and do not evaluate whether the actuators are truly optimal. A key gap remains in explicitly accounting for gearbox mass and efficiency and in automating planetary gearbox design to systematically optimize 3D-printed actuators.

To address these challenges, we present **COMPAct: Computational Optimization and automated Modular**

---

* These authors have contributed equally.

Parametric Design of 3D-Printed Planetary Actuators, a unified optimization and automation framework, see Fig.1. The key contributions are:

1) **Gearbox optimization:** We present an optimization framework for four types of planetary gearboxes. The framework minimizes actuator mass and width while maximizing efficiency using a detailed mass model.
2) **CAD automation:** Automated parametric CAD models are generated, enabling direct 3D printing of optimized actuators without requiring manual redesign.
3) **Hardware validation:** Two actuators from the framework, an SSPG (MN8014 motor, 7.2:1) and a CPG (MAD M6C12 motor, 14:1), are fabricated and experimentally tested to validate the proposed approach.

The framework supports four gearbox types: Single-Stage (SSPG), Compound (CPG), Wolfrom/3K (WPG), and Double-Stage (DSPG).

The remainder of this paper is organized as follows. Section II introduces the gearbox designs and mass model. Section III formulates the optimization problem, and Section IV describes the automation framework. Section V presents the optimization outcomes, CAD automation, and hardware validation. Finally, Section VI concludes the paper and outlines directions for future work.

II. GEARBOX DESIGNS

This section introduces the gearbox architectures analyzed to identify the optimal actuator, along with their gear ratio and efficiency expressions. A unified notation for gear parameters is used for consistency (see Section III-A). Only relevant variables are active; e.g., SSPG uses stage-1 parameters only, while CPG and WPG omit certain gears in stage-1 or stage-2. Gear ratios are derived from standard planetary gear equations [27], and efficiency expressions follow the analysis in [28] using basic driving efficiencies from [29].

A. Single Stage Planetary Gearbox (SSPG)

The single-stage planetary gearbox (SSPG) considered in this work has the ring gear fixed, the sun gear driven by the motor, and the carrier providing the output, see Fig. 2. This arrangement provides the highest gear reduction among planetary configurations. The gear reduction ratio of the SSPG is given by

$$G_{\text{SSPG}} = \frac{\omega_s}{\omega_c} = \frac{N_{s_1} + N_{r_1}}{N_{s_1}}, \tag{1}$$

where G_{SSPG} is the gear reduction ratio, ω_c is the angular velocity of the carrier (output) shaft, ω_s is the angular velocity of the sun gear (input) shaft, N_{s_1} is the number of teeth on the sun gear, and N_{r_1} is the number of teeth on the ring gear.

The efficiency of the SSPG is expressed as

$$\eta_{\text{SSPG}} = \frac{N_{s_1} + \eta_{s_1 p_1} \eta_{p_1 r_1} N_{r_1}}{N_{s_1} + N_{r_1}}, \tag{2}$$

where η_{SSPG} is the overall efficiency of the gearbox, $\eta_{s_1 p_1}$ denotes the efficiency of the sun–planet gear mesh, and $\eta_{p_1 r_1}$ denotes the efficiency of the planet–ring gear mesh.
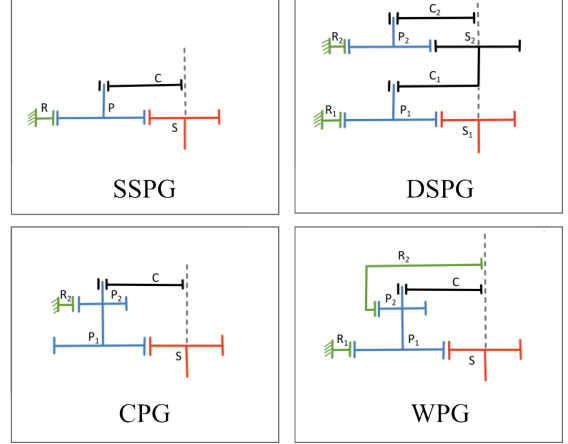

Fig. 2: Line diagrams of planetary gearbox configurations. **SSPG:** Sun (S) input, Ring (R) fixed, Carrier (C) output. **CPG:** Sun (S) input, Ring (R_2) fixed, Carrier (C) output; planets (P_1, P_2) rigidly attached. **DSPG:** Sun (S_1) input, Rings (R_1, R_2) fixed, Carrier (C_2) output; S_2 and C_1 rigidly attached. **WPG (3K):** Sun (S) input, Ring (R_1) fixed, Ring (R_2) output; planets (P_1, P_2) rigidly attached.

B. Compound Planetary Gearbox (CPG)

The compound planetary gearbox (CPG) considered here uses compound planet gears, each comprising two rigidly connected gears of different diameters. In this configuration, the sun gear drives the larger planet, while the smaller planet meshes with a fixed ring gear (Fig. 2). For simplicity, the sun and larger planet module m_1, is equal to the smaller planet and ring module m_2.

The gear reduction ratio of the CPG is

$$G_{\text{CPG}} = \frac{(N_{s_1} + N_{p_1})(N_{p_2} + N_{p_1})}{N_{s_1} N_{p_2}}, \tag{3}$$

where G_{CPG} is the gear reduction ratio, N_{s_1} is the number of teeth on the sun gear, N_{p_1} and N_{p_2} are the numbers of teeth on the larger and smaller planet gears, respectively, and N_{r_2} is the number of teeth on the ring gear.

The efficiency of the CPG is

$$\eta_{\text{CPG}} = \frac{N_{s_1} N_{p_2} + \eta_{s_1 p_1} \eta_{p_2 r_2} N_{p_1} N_{r_2}}{(N_{s_1} + N_{p_1})(N_{p_2} + N_{p_1})}, \tag{4}$$

where η_{CPG} is the overall efficiency, $\eta_{s_1 p_1}$ is the sun–planet mesh efficiency, and $\eta_{p_2 r_2}$ is the planet–ring mesh efficiency.

C. Double-Stage Planetary Gearbox (DSPG)

The double-stage planetary gearbox (DSPG) employs two successive planetary layers to achieve high gear reductions, see Fig. 2. Although less efficient due to the added stages, it is included in this work for its ability to provide exceptionally large gear ratios.

The gear reduction ratio of the DSPG is

$$G_{\text{DSPG}} = G_{\text{DSPG}}^1 G_{\text{DSPG}}^2 = \prod_{i=1}^{2} \frac{N_{s_i} + N_{r_i}}{N_{s_i}}, \tag{5}$$

where G_{DSPG} is the overall gear reduction ratio, G^i_{DSPG} is the ratio of the ith stage, N_{s_i} is the number of teeth on the sun gear, and N_{r_i} is the number of teeth on the ring gear in stage i. The overall efficiency of the DSPG is

$$\eta_{\text{DSPG}} = \eta^1_{\text{DSPG}} \eta^2_{\text{DSPG}} = \prod_{i=1}^{2} \frac{N_{s_i} + \eta_{s_i p_i}\, \eta_{p_i r_i}\, N_{r_i}}{N_{s_i} + N_{r_i}}, \quad (6)$$

where η_{DSPG} is the overall efficiency, η^i_{DSPG} the efficiency of the ith stage, $\eta_{s_i p_i}$ the sun–planet mesh efficiency, and $\eta_{p_i r_i}$ the planet–ring mesh efficiency.

D. Wolfrom (3K) Planetary Gearbox (WPG)

The Wolfrom (3K) planetary gearbox (WPG) [28] is a specialized transmission topology designed to achieve very high gear reductions within a compact volume. Its architecture consists of a sun gear (S) driven by the motor, two rigidly connected planet gears (P_1 and P_2), and two concentric ring gears (R_1 and R_2). In the configuration considered in this work, the input is applied to the sun gear S, the first ring gear R_1 is fixed, and the second ring gear R_2 provides the output, see Fig. 2. The gear reduction ratio of the WPG is

$$G_{\text{WPG}} = \frac{1 + I_1}{1 - I_2}, \quad (7)$$

where

$$I_1 = \frac{N_{r_1}}{N_{s_1}}, \qquad I_2 = \frac{N_{r_1} N_{p_2}}{N_{p_1} N_{r_2}}. \quad (8)$$

Here, N_{s_1} and N_{r_1} are the numbers of teeth on the sun gear S and ring gear R_1, respectively, N_{p_1} and N_{p_2} are the teeth numbers of planets P_1 and P_2, and N_{r_2} is the number of teeth on the output ring gear R_2.

The efficiency of the WPG is

$$\eta_{\text{WPG}} = \frac{\eta_{p_2 r_2} \left(\eta_{p_1 r_1} + \eta_{s_1 p_1} I_1 \right) \left(1 - I_2 \right)}{\left(1 + I_1 \right) \left(\eta_{p_1 r_1} \eta_{p_2 r_2} - I_2 \right)}, \quad (9)$$

where η_{WPG} is the overall efficiency, $\eta_{s_1 p_1}$ the sun–planet (S–P_1) mesh efficiency, $\eta_{p_1 r_1}$ the planet–ring (P_1–R_1) mesh efficiency, and $\eta_{p_2 r_2}$ the planet–ring (P_2–R_2) mesh efficiency.

E. Actuator Mass Model

To obtain actuator masses close to real values, we developed a detailed model accounting for every component. Each part is decomposed into simple geometries (cylinders, shells, cones). For example, a planetary gear in the CPG is modeled as two cylinders, with diameters and heights corresponding to the pitch circle diameters and face widths of Planet 1 and Planet 2. Using this approach, all components are approximated by suitable geometry combinations, as detailed in our repository. Predicted masses are compared with CAD-based estimates in Fig. 5. Bearings, nuts, and bolts are selected from standard datasheets for accessibility and ease of assembly.

III. OPTIMIZATION OF THE GEARBOX

This section presents the optimization problem formulation for the actuator gearbox. The following subsections define the design variables for different gearbox configurations, specify the governing constraints, and describe the objective functions.

A. Optimization Variables

A unified notation is used for all gearbox types (SSPG, CPG, WPG, DSPG). The design variables are common across configurations and collected in vector $X \in \mathcal{X} \subseteq \mathbb{R}^{10}$:

$$X := [N^s_1, N^p_1, N^r_1, N^s_2, N^p_2, N^r_2, m_1, m_2, n^p_1, n^p_2], \quad (10)$$

where N^s_i, N^p_i, N^r_i are the sun, planet, and ring gear teeth counts, m_i is the module, and n^p_i the number of planets in stage i ($i \in \{1, 2\}$). All variables are integers except m_i, which is chosen from a discrete set. Not all gearboxes use both stages. In SSPG, stage 2 is absent ($N^s_2, N^p_2, N^r_2, m_2, n^p_2 = 0$). In CPG, $N^r_1 = 0$ and $N^s_2 = 0$. In WPG, $N^s_2 = 0$. In both CPG and WPG, planets are rigidly attached, so $n^p_1 = n^p_2$. DSPG has no such restrictions.

B. Constraints

To ensure feasibility and manufacturability, the optimization problem includes several classes of constraints, described below.

I. **Gear Ratio Constraint:** The gear ratio of all the types of gearboxes are discussed in Section II. The following constraint ensures it remains within the specified range:

$$GR_{min} \leq GR \leq GR_{max} \quad (11)$$

II. **Geometric Constraints:** These constraints enforce dimensional compatibility between the sun, planet, and ring gears within each stage. The conditions [30] for different gearbox types are:

$$
\begin{aligned}
\text{SSPG/DSPG:} \quad & N^r_i = N^s_i + 2N^p_i, \\
\text{CPG:} \quad & m_2 N^r_2 = m_1(N^s_1 + N^p_1) + m_2 N^p_2, \\
\text{WPG:} \quad & N^r_1 = N^s_1 + 2N^p_1, \\
& m_2 N^r_2 = m_1(N^s_1 + N^p_1) + m_2 N^p_2, \\
& m_2 N^r_2 > m_1 N^r_1.
\end{aligned}
\quad (12)
$$

The additional inequality in the WPG ensures that the stage-2 ring gear is larger than the stage-1 ring gear. This configuration enables higher gear reduction for the same available space, thereby achieving a more torque-dense design (see Section II-D).

III. **Meshing Constraints:** These constraints enforce proper tooth engagement between gears in each configuration [30]. They are expressed using the modulo operator, where $a \ \% \ b = 0$ indicates that a is divisible by b:

$$
\begin{aligned}
\text{SSPG/DSPG:} \quad & (N^s_i + N^r_i) \ \% \ n^p_i = 0, \\
\text{CPG:} \quad & N^s_1 \ \% \ n^p_1 = 0, \quad N^r_2 \ \% \ n^p_1 = 0, \\
\text{WPG:} \quad & (N^s_1 + N^r_1) \ \% \ n^p_1 = 0, \\
& N^s_1 \ \% \ n^p_1 = 0, \\
& N^r_2 \ \% \ n^p_1 = 0.
\end{aligned}
\quad (13)
$$

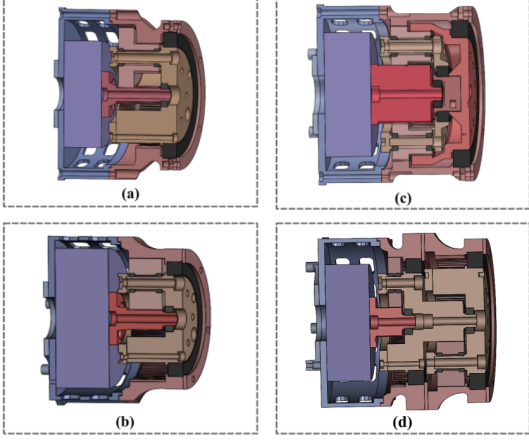For CPG and WPG, the planets are rigidly connected across stages, hence $n^p_1 = n^p_2$.

Fig. 3: 3D CAD models of the actuators (Red: **gear assembly**, Blue: **motor assembly**). (a) **CPG:** 14:1, Motor: MAD-M6C12; (b) **SSPG:** 7.2:1, Motor: T-motor MN8014; (c) **WPG:** 16.36:1, Motor: MAD-M6C12; (d) **DSPG:** 22.05:1, Motor: MAD-M6C12. Refer Table I for specifications.

IV. **No Interference Constraints:** These constraints prevent collisions between adjacent planet gears and the carrier extrusion. The conditions are formulated using pitch radii [30]:

$$\text{SSPG/DSPG:} \quad 2(R_i^s + R_i^p)\sin\left(\frac{\pi}{2n_i^p}\right) - R_i^p - R_{ce} \geq \delta_{ce},$$

$$\text{CPG/WPG:} \quad 2(R_1^s + R_1^p)\sin\left(\frac{\pi}{2n_1^p}\right) - R_1^p - R_{ce} \geq \delta_{ce}. \tag{14}$$

Here, R_i^s and R_i^p are the pitch radii of the sun and planet gears in stage i, $R_{ce} = 4$ mm is the carrier extrusion radius, and $\delta_{ce} = 1$ mm is the minimum clearance required to avoid interference.

V. **Maximum Outer Gearbox Diameter Constraints:** These constraints limit the maximum outer diameter of the gearbox. For SSPG, WPG and DSPG, the ring gear diameter must not exceed $D_{GB}^{\max}$, while in CPG the outermost point of the larger planet gear must remain within $D_{GB}^{\max}$.

$$\text{SSPG/DSPG/WPG:} \quad m_i N_i^r + \delta_{rw} \leq D_{GB}^{\max},$$
$$\text{CPG:} \quad m_1(N_1^s + 2N_1^p) \leq D_{GB}^{\max}. \tag{15}$$

Here, δ_{rw} is the radial width of the ring gear (taken as 5 mm in this work). The maximum gearbox diameter is defined as $D_{GB}^{\max} = K_{mgd}D_{motor}$, where K_{mgd} is a user-defined hyperparameter specifying the allowable gearbox-to-motor diameter ratio.

VI. **Additional Constraints:** These constraints restrict the feasible ranges of the design variables:

$$m_{\min} \leq m_i \leq m_{\max}, \quad N_i^s, N_i^p \geq N_{\min},$$
$$n_p^{\min} \leq n_i^p \leq n_p^{\max}. \tag{16}$$

Some variables are fixed to zero depending on the gearbox type (see Section III-A) and will not follow these constraints; their separate formulations are excluded for brevity. In this work, we use $m_{\min} = 0.5$ mm, $m_{\max} = 1.2$ mm, and $N_{\min} = 18$ to avoid undercutting. The number of planet gears is constrained to $n_p \in [2, 7]$ following standard practice.

C. Optimization Formulation

The objective is to minimize actuator mass, maximize gearbox efficiency, and reduce axial width while satisfying a target gear ratio or range. Actuator mass M_{act} is computed as in Section II-E, and efficiency η as in Section II. Gear widths are derived from the modified Lewis strength equation [31], while overall actuator width W_p is primarily set by gearbox width, since motor and bearing lengths remain fixed. W_p is therefore included in the cost function to penalize excessive axial dimensions. For a specific ratio GR_{req}, a penalty weighted by K_g accounts for deviation between GR and GR_{req}. Equivalently, bounds can be set as $GR_{\min} = GR_{req} - 1$ and $GR_{\max} = GR_{req} + 1$. For ratio ranges, $K_g = 0$ with limits $[GR_{\min}, GR_{\max}]$. The cost function is

$$C_{\text{act}} := K_m M_{act} - K_e \eta + K_w W_p + K_g |GR_{req} - GR| \tag{17}$$

where K_m, K_e, K_w, and K_g weight mass, efficiency, width, and ratio tracking. The optimization problem is

$$\min_{\mathcal{X}} \quad C_{\text{act}}$$
$$\text{s.t.} \quad \text{Constraints I–VI.} \tag{18}$$

The solution C_{act}^* gives the minimum cost for a specified gear ratio or gear ratio range. Since all variables are discrete, the problem is solved via brute-force search by evaluating all feasible values in the constraint set. This guarantees the global optimum but is more computationally expensive than other methods. In practice, runtimes remain modest: SSPG converges in a fraction of a second, CPG and WPG in under five seconds, and DSPG within a few minutes, for a given gear-ratio for each gearbox type.

IV. AUTOMATION OF ACTUATOR DESIGN

1) Actuator Design: Each actuator is modular, comprising a *motor subassembly* (motor, casing, driver) and a *gearbox subassembly* (gears and carriers, varying by type), as shown in Fig. 3. To improve durability of 3D-printed parts, the sun gear shaft is reinforced with a central bolt, and the motor casing incorporates through-bolts that act as a structural skeleton, enhancing housing stiffness.

2) Motor and Motor Driver Selection: The COMPAct framework accepts different motors and drivers as inputs to generate CAD designs. The optimization and automation pipeline uses the motor's theoretical torque capacity to determine gear width, while motor and driver dimensions are treated as fixed design dimensions (see Section IV-.3). In our study, we use T-Motor (U8, U10, U12, MN8014), MAD M6C12, and Vector 8020 motors with ODrive Pro and Moteus drivers. Additional motors and drivers can be integrated by providing their dimensions and torque–power data.

3) Automation of Actuator Design: The actuator design process was automated using *parametric CAD modeling*, linking optimization variables directly to geometric dimensions. All design parameters were defined as CAD variables, updated by the optimization program, and grouped as: (i) **Optimization variables** (e.g., gear teeth, module, planet count); (ii) **Fixed dimensions** (motor casing, clearances, hole sizes); and (iii) **Dependent dimensions** (functions of the first two). Optimization yields the optimal teeth numbers, module, and planet count, which update the CAD model. Together with fixed dimensions, they define the dependent dimensions, ensuring automatic updates. The parametric model was designed to avoid interference and assembly conflicts across gear ratios and configurations.

4) Integration with Optimization Framework: The communication between the optimization algorithm and the CAD model is managed through a *text-based variable file*. All design variables, including optimization, fixed, and dependent, are stored in this file, which is linked to the CAD environment. Whenever the optimization program updates the file, the CAD model is automatically refreshed to reflect the new design. For the four gearbox architectures investigated, namely SSPG, CPG, WPG, and DSPG, the total number of design variables defined in the framework is approximately **150 for each type**.

5) Customization and Hyperparameters: The automation framework also allows user-level customization through both fixed design parameters and optimization hyperparameters. Examples of fixed design variables include motor outer casing thickness, clearances between components, mounting plate thickness, and hole diameters. In addition, hyperparameters such as the maximum allowable gearbox diameter, motor selection, motor driver configuration, and variable bounds for optimization can be modified to suit different design requirements.

V. RESULTS

A. Simulation Results

This study evaluates the capability of the proposed framework to identify optimal actuator parameters and gearbox types for a given motor. The MAD M6C12 motor was used for the analysis. Optimal gearbox designs were generated for gear ratios ranging from 4:1 to 60:1 in unit increments (e.g., 4:1–5:1, 5:1–6:1, …, 59:1–60:1) across four gearbox types: SSPG, CPG, DSPG, and WPG. The actuator mass, efficiency, width, and cost were computed for each case, and the results are summarized in Figs. 5 and 6.

1) Validation of the Mass Model: The accuracy of the actuator mass model used in the optimization framework was assessed by comparing its predictions against masses obtained from automated parametric CAD models. The root-mean-square (RMS) error between the two estimates was computed for each gearbox type. As shown in Fig. 5, the difference between the model and CAD-based calculations is minimal. The RMS error for SSPG, CPG, DSPG and WPG is 0.01 kg, 0.005 kg, 0.024 kg, and 0.028 kg, respectively. These results confirm that the proposed mass model closely
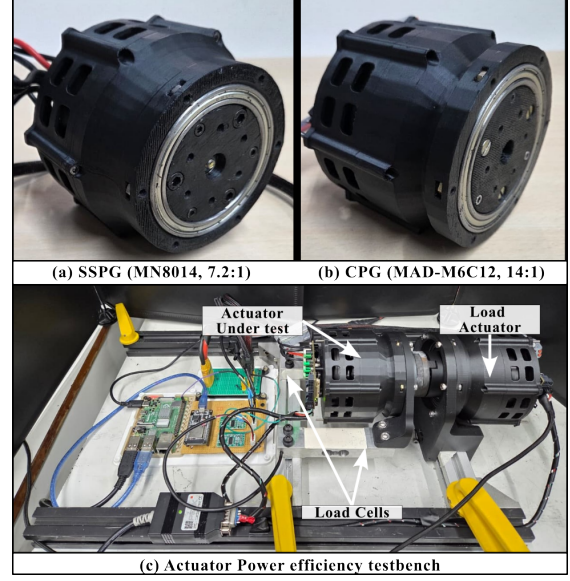

Fig. 4: (a) **Assembled SSPG actuator**, (b) **Assembled CPG actuator**, (c) **Power efficiency testbench**: two load cells measure the torque of the actuator under test, while a second actuator serves as the load.
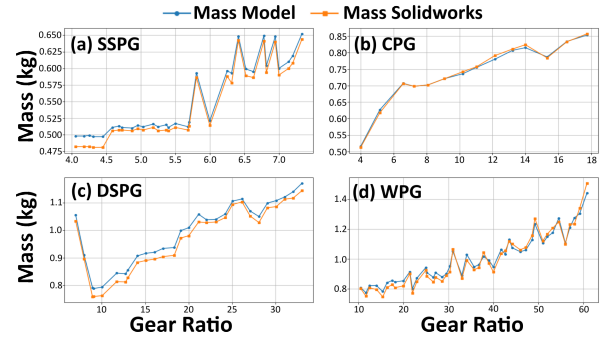

Fig. 5: Comparison of mass model predictions with 3D CAD estimates. The model closely matches the final CAD masses, with RMS errors of 0.01 kg (SSPG), 0.005 kg (CPG), 0.024 kg (DSPG), and 0.028 kg (WPG).

approximates the real actuator mass, thereby strengthening the reliability of the optimization framework.

2) Optimal Gearbox Designs: The framework was further used to compare gearbox types and identify the most suitable designs across the specified ratio range. The following observations can be made from Fig. 6:

1) The feasible design space varies significantly. SSPG is limited to ratios up to 7.2:1, CPG to 18:1, DSPG to 32:1, while only WPG spans the full 4:1–60:1 range.
2) In the 4:1–7.2:1 range, SSPG offers the lowest cost, while also being the lightest, most efficient, and most compact actuator.
3) Between 7.2:1 and 15:1, CPG emerges as the optimal option, with a cost advantage and efficiency nearly comparable to SSPG.
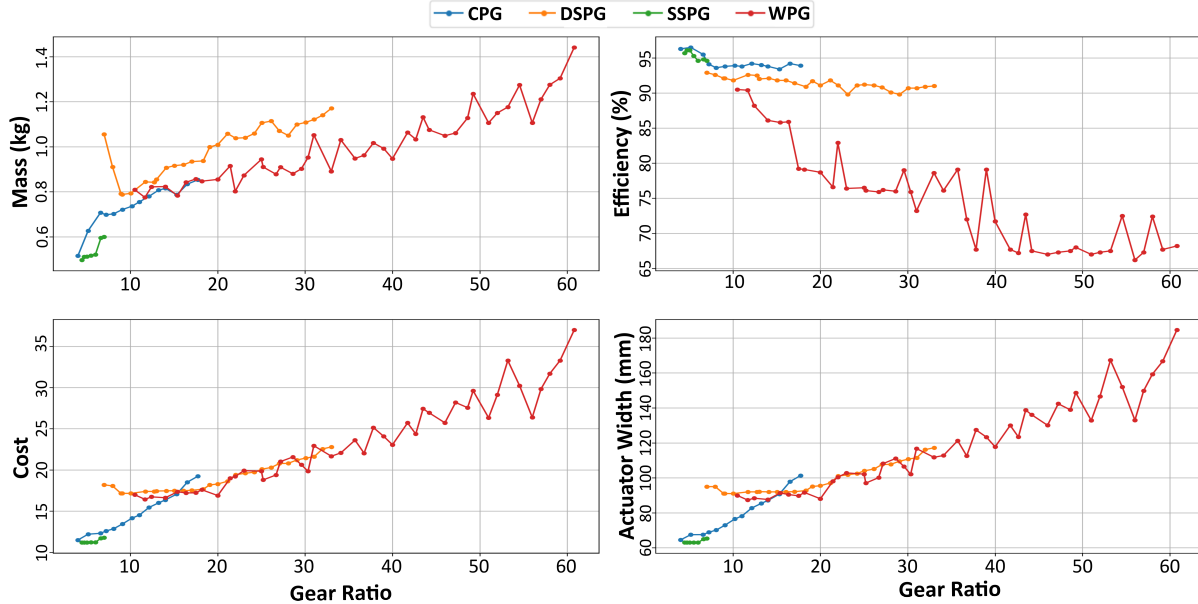4) In the 15:1–32:1 range, WPG and DSPG are closely competing, with DSPG showing higher efficiency. Be-

Fig. 6: Optimization results for gearbox ratios between 4:1–60:1 with the MAD-M6C12 motor. Mass, efficiency, width, and cost are plotted against gear ratio to identify the optimal gearbox type for a given motor.

yond 32:1, only WPG remains feasible.

These results highlight the utility of the COMPAct framework in validating design models and supporting informed actuator selection across a wide range of applications. For example, when selecting a gearbox with the MAD-M6C12 motor in the 14–15:1 ratio range, the framework identifies the CPG as the optimal solution (minimum cost), with the corresponding parameters listed in Table I. The framework also automates CAD generation of the selected design, as illustrated in Fig. 3. While the framework produces detailed optimal parameters for all gearboxes, only representative results for selected cases are reported in Table I for brevity.

B. Hardware Results

Using the automation framework, four optimal actuators are designed (Fig. 3). The SSPG and CPG are 3D-printed and experimentally tested. The **SSPG actuator** uses an MN8014 motor (87.8 mm OD), whereas the **CPG actuator** employs a MAD M6C12 motor (72 mm OD). Accordingly, the hyperparameter K_{mgd} in Eq. (15) is set to 1 for SSPG and 1.25 for CPG.

1) Power Efficiency Test: The power efficiency of the actuators was evaluated on a custom-built dynamometer, similar to the setup in Berkeley Humanoid Lite [23] (Fig. 4). The test actuator was run in torque-control mode, while the load actuator was velocity-controlled to maintain constant speed. Electrical input power was computed as supply voltage times current, and mechanical output power as output angular velocity times measured torque. Angular velocity was obtained from the motor encoder (scaled by gear reduction), and torque from load cells integrated into the mount. Mechanical efficiency, representing gearbox transmission efficiency, was defined as mechanical output power

TABLE I: Optimized Actuator Designs from the COMPAct Framework

Actuator (Motor)	Gear Ratio (Range)	Optimal Parameters $[N_i^s, N_i^p, N_i^r, m_i, n_i^p]\ i \in \{1, 2\}$	
SSPG (MN8014)	7.2:1 (7.2–7.3:1)	**Stage-1:** $[25, 65, 155, 0.5, 3]$ **Stage-2:** $[0, 0, 0, 0, 0]$	
CPG (M6C12)	14:1 (14–15:1)	**Stage-1:** $[18, 66, 0, 0.6, 3]$ **Stage-2:** $[0, 33, 117, 0.6, 3]$	
DSPG (M6C12)	22.05:1 (22–23:1)	**Stage-1:** $[35, 52, 139, 0.5, 3]$ **Stage-2:** $[23, 28, 79, 1.0, 3]$	
WPG (M6C12)	16.36:1 (16–17:1)	**Stage-1:** $[66, 45, 156, 0.5, 6]$ **Stage-2:** $[0, 33, 144, 0.5, 6]$	

Notes: 1) Zero values indicate non-existent gears/parameters in that stage. 2) In CPG and WPG, the two planet sets (p_1, p_2) are rigidly connected, hence the number of planets is equal across stages.

over commanded torque–velocity product. Overall actuator efficiency was defined as mechanical output power over electrical input power, thus accounting for motor Joule losses, driver efficiency, and bearing losses. Tests were performed at five angular velocities and torques up to 18 Nm. For each pair, the actuator was ramped to the target and held for 10s, with analysis based on steady-state data. The efficiency results are presented in Fig.7. The optimization framework predicted efficiencies of 96% for SSPG and 93.8% for CPG. Experimentally, the mechanical efficiency was lower: 60–80% for SSPG and about 60% for CPG. This discrepancy is attributed to deviations from the ideal involute tooth profile caused by 3D-printing resolution limits. Also, the lack of industrial-grade precision in 3D-printed parts introduces additional friction in the gear system. Nonetheless, SSPG consistently outperformed CPG, consistent with theoretical predictions. Total efficiency increased with angular velocity, while mechanical efficiency remained velocity-independent.
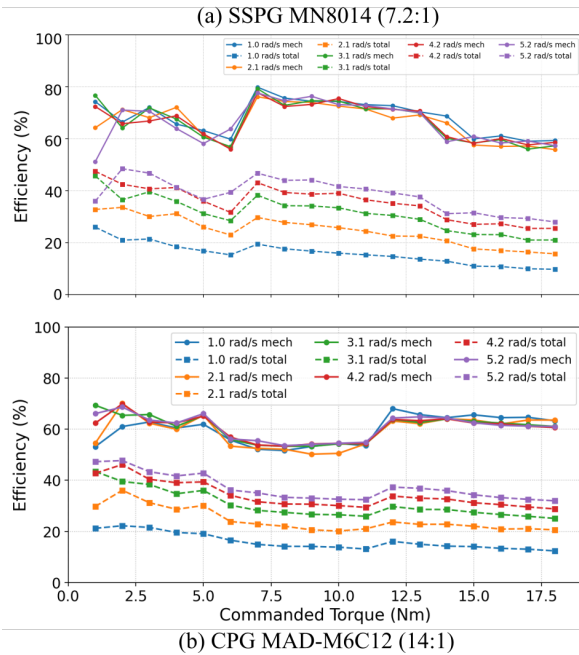
(a) SSPG MN8014 (7.2:1)

(b) CPG MAD-M6C12 (14:1)

Fig. 7: Efficiency of SSPG (top) and CPG (bottom). Mechanical efficiency (solid lines) is measured power over commanded torque–velocity product, while total efficiency (dotted lines) is measured power over electrical input power.
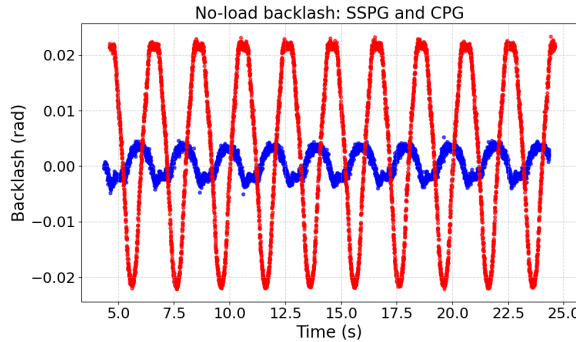

Fig. 8: No-load backlash test results. The compound planetary gearbox (CPG, red) exhibits a backlash of 0.046 rad (2.6°), whereas the single-stage planetary gearbox (SSPG, blue) shows a lower backlash of 0.010 rad (0.59°)

At higher torques, total efficiency decreased, likely due to greater Joule losses.

2) No-Load Backlash Test: The no-load backlash of SSPG (7.2:1) and CPG (14:1) was measured using two encoders: the motor-side encoder (integrated in the driver) and a high-resolution output encoder. A low-frequency, small-amplitude sinusoidal velocity ensured smooth motion while neglecting gearbox compliance. The motor angle θ_m was scaled by the gear ratio G to compare with the output angle θ_o, and the relative motion was computed as $\Delta\theta(t) = \frac{\theta_m(t)}{G} - \theta_o(t)$. Backlash was estimated as $\beta = \max_t \Delta\theta(t) - \min_t \Delta\theta(t)$.

The measured values were $\beta_{\text{SSPG}} = 0.010$ rad (0.59°) and $\beta_{\text{CPG}} = 0.046$ rad (2.6°), as shown in Fig. 8. The CPG

TABLE II: Estimated stiffness values.

	Forward	Backward	**Mean** (K)
SSPG (7.2:1)	238.4	247.0	**242.7 [Nm/rad]**
CPG (14:1)	211.0	192.2	**201.6 [Nm/rad]**

exhibited higher backlash, likely due to the smaller effective planet diameters in its second stage, which reduce contact ratio and increase clearance.
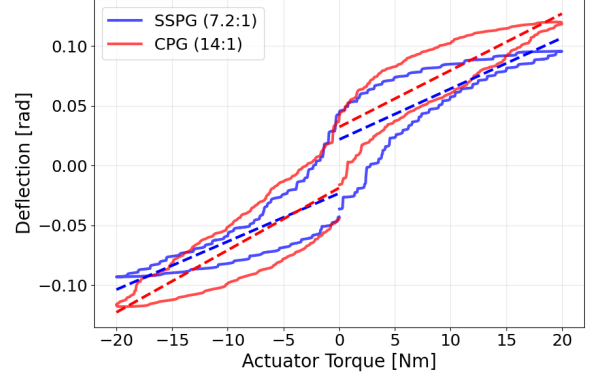

Fig. 9: Transmission stiffness: The x-axis shows the commanded actuator torque at the output, and the y-axis indicates the internal deflection. The CPG (red) exhibits lower stiffness than the SSPG (blue).

3) Transmission Stiffness: Transmission stiffness was measured for SSPG (7.2:1) and CPG (14:1). The actuator output was rigidly fixed, and a motor torque command was applied: ramping from 0 to ±20 Nm and back. Motor encoder readings were divided by the gear ratio to obtain internal deflection. For each actuator, linear fits were applied separately to the positive and negative torque samples, $\theta = \frac{\tau}{K} + b$, where θ is deflection, τ the applied torque, K the stiffness, and b a bias term. The reported stiffness is the mean of the two estimates. Results (Fig. 9) show hysteresis, consistent with prior reports on 3D-printed transmissions in Humanoid Lite [23] and Roozing et. al. [32]. Measured stiffness values (Table II) were 242.7 Nm/rad for SSPG and 201.6 Nm/rad for CPG. For comparison, Roozing [32] reported 1468 Nm/rad and Humanoid Lite [23] 319 Nm/rad. Higher values in these works likely result from cycloidal transmissions (larger contact areas) and stronger materials (e.g., carbon-fiber–reinforced polyamide versus PLA in our prototypes). In our tests, CPG stiffness was lower than SSPG, attributed to the smaller planet diameter in its second stage, which reduces contact ratio and effective stiffness.

VI. CONCLUSION

This paper presented **COMPAct**, a framework for computational optimization and automated modular design of 3D-printed planetary actuators. By combining gearbox parameter optimization with CAD automation, the framework enables rapid design exploration and fabrication. Simulations identified feasible gearbox designs across four types, SSPG, CPG, DSPG, and WPG, while validation against CAD models

confirmed the accuracy of the mass model. Automatic CAD generation further supports seamless transition from optimization to fabrication. To demonstrate practicality, two actuators were fabricated and tested for power efficiency, transmission stiffness, and backlash, confirming the framework's ability to produce lightweight and manufacturable designs. Future work includes extending the framework to additional gearbox types, such as cycloidal drives, conducting extensive endurance tests across all actuator types, evaluating power efficiency with more reliable torque sensing, adapting the framework for metal-based actuators, and, reducing the optimization computational time by using better optimizations than brute force, like MINLP solvers.

REFERENCES

[1] K. M. Digumarti, C. Gehring, S. Coros, J. Hwangbo, and R. Siegwart, "Concurrent optimization of mechanical design and locomotion control of a legged robot," in *Mobile Service Robotics*. World Scientific, 2014, pp. 315–323.

[2] G. Fadini, S. Kumar, R. Kumar, T. Flayols, A. Del Prete, J. Carpentier, and P. Souères, "Co-designing versatile quadruped robots for dynamic and energy-efficient motions," *Robotica*, vol. 42, no. 6, p. 2004–2025, 2024.

[3] M. Chadwick, H. Kolvenbach, F. Dubois, H. F. Lau, and M. Hutter, "Vitruvio: An open-source leg design optimization toolbox for walking robots," *IEEE Robotics and Automation Letters*, vol. 5, no. 4, pp. 6318–6325, 2020.

[4] Á. Belmonte-Baeza, J. Lee, G. Valsecchi, and M. Hutter, "Meta reinforcement learning for optimal design of legged robots," *IEEE Robotics and Automation Letters*, vol. 7, pp. 12 134–12 141, 2022. [Online]. Available: https://api.semanticscholar.org/CorpusID: 252732294

[5] S. Ha, S. Coros, A. Alspach, J. Kim, and K. Yamane, "Joint optimization of robot design and motion parameters using the implicit function theorem," *Robotics: Science and Systems XIII*, 2017. [Online]. Available: https://api.semanticscholar.org/CorpusID:2672904

[6] G. Bravo-Palacios, A. D. Prete, and P. M. Wensing, "One robot for many tasks: Versatile co-design through stochastic programming," *IEEE Robotics and Automation Letters*, vol. 5, no. 2, pp. 1680–1687, 2020.

[7] G. Bravo-Palacios, G. Grandesso, A. D. Prete, and P. M. Wensing, "Robust co-design: Coupling morphology and feedback design through stochastic programming," *Journal of Dynamic Systems, Measurement, and Control*, vol. 144, no. 2, p. 021007, Nov. 2021.

[8] T. Dinev, C. Mastalli, V. Ivan, S. Tonneau, and S. Vijayakumar, "A versatile co-design approach for dynamic legged robots," in *2022 IEEE/RSJ International Conference on Intelligent Robots and Systems (IROS)*, 2022, pp. 10 343–10 349.

[9] G. Fadini, T. Flayols, A. Del Prete, N. Mansard, and P. Souères, "Computational design of energy-efficient legged robots: Optimizing for size and actuators," in *2021 IEEE International Conference on Robotics and Automation (ICRA)*, 2021, pp. 9898–9904.

[10] G. Fadini, T. Flayols, A. D. Prete, and P. Souères, "Simulation aided co-design for robust robot optimization," *IEEE Robotics and Automation Letters*, vol. 7, no. 4, pp. 11 306–11 313, 2022.

[11] Y. Ding and H.-W. Park, "Design and experimental implementation of a quasi-direct-drive leg for optimized jumping," in *2017 IEEE/RSJ International Conference on Intelligent Robots and Systems (IROS)*, 2017, pp. 300–305.

[12] Y.-H. Shin, S. Hong, S. Woo, J. Choe, H. Son, G. Kim, J.-H. Kim, K. Lee, J. Hwangbo, and H.-W. Park, "Design of kaist hound, a quadruped robot platform for fast and efficient locomotion with mixed-integer nonlinear optimization of a gear train," in *2022 International Conference on Robotics and Automation (ICRA)*, 2022, pp. 6614–6620.

[13] J. Choe, G. Kim, H. Kim, D. Kang, M.-S. Kim, and H.-W. Park, "Design of a 3-dof hopping robot with an optimized gearbox: An intermediate platform toward bipedal robots," 2025. [Online]. Available: https://arxiv.org/abs/2505.12231

[14] R. Wu, C. Xiao, and C. Zheng, "Deepcad: A deep generative network for computer-aided design models," 2021. [Online]. Available: https://arxiv.org/abs/2105.09492

[15] Y. Du, S. Chen, W. Zan, P. Li, M. Wang, D. Song, B. Li, Y. Hu, and B. Wang, "Blenderllm: Training large language models for computer-aided design with self-improvement," 2024. [Online]. Available: https://arxiv.org/abs/2412.14203

[16] J. D. Camba, M. Contero, and P. Company, "Parametric cad modeling: An analysis of strategies for design reusability," *Computer-Aided Design*, vol. 74, pp. 18–31, 2016. [Online]. Available: https://www.sciencedirect.com/science/article/pii/S0010448516000051

[17] D. Roller, "An approach to computer-aided parametric design," *Computer-Aided Design*, vol. 23, no. 5, pp. 385–391, 1991. [Online]. Available: https://www.sciencedirect.com/science/article/pii/001044859190033S

[18] *A Full Parametric Model for Turbomachinery Blade Design and Optimisation*, ser. International Design Engineering Technical Conferences and Computers and Information in Engineering Conference, vol. Volume 1: 30th Design Automation Conference, 09 2004. [Online]. Available: https://doi.org/10.1115/DETC2004-57467

[19] M. Fürst, J. Götz, M. Otto, and K. Stahl, "Automation of gearbox design," *Forschung im Ingenieurwesen*, vol. 86, no. 3, pp. 409–420, 2022. [Online]. Available: https://doi.org/10.1007/s10010-021-00517-3

[20] K. Urs, C. E. Adu, E. J. Rouse, and T. Y. Moore, "Design and characterization of 3d printed, open-source actuators for legged locomotion," 2022. [Online]. Available: https://arxiv.org/abs/2202.12395

[21] T. Yoshida, G. Endo, A. Okubo, and H. Nabae, "Experimental evaluation of a quasi-direct-drive actuator with a 3d-printed planetary gear reducer," in *2023 IEEE/SICE International Symposium on System Integration (SII)*, 2023, pp. 1–6.

[22] R. Bezzini, G. Bassani, C. A. Avizzano, and A. Filippeschi, "Design and experimental evaluation of multiple 3d-printed reduction gearboxes for wearable exoskeletons," *Robotics*, vol. 13, no. 11, 2024. [Online]. Available: https://www.mdpi.com/2218-6581/13/11/168

[23] Y. Chi, Q. Liao, J. Long, X. Huang, S. Shao, B. Nikolic, Z. Li, and K. Sreenath, "Demonstrating berkeley humanoid lite: An open-source, accessible, and customizable 3d-printed humanoid robot," 2025. [Online]. Available: https://arxiv.org/abs/2504.17249

[24] F. Grimminger, A. Meduri, M. Khadiv, J. Viereck, M. Wüthrich, M. Naveau, V. Berenz, S. Heim, F. Widmaier, T. Flayols, J. Fiene, A. Badri-Spröwitz, and L. Righetti, "An open torque-controlled modular robot architecture for legged locomotion research," *IEEE Robotics and Automation Letters*, vol. 5, no. 2, pp. 3650–3657, 2020.

[25] N. Twersky, "3d printed qdd robotic actuator (mit mini cheetah clone)," https://www.instructables.com/3D-Printed-QDD-Robotic-Actuator-MIT-Mini-Cheetah-C/, 2025, accessed: 2025-09-07.

[26] G. Levine, "Opentorque actuator," https://hackaday.io/project/159404-opentorque-actuator, 2018, accessed: 2025-09-07.

[27] J. G. R.S. Khurmi, *Theory of Machines and Mechanism*, vol 1 ed. S.CHAND and COMPANY LTD, 2015.

[28] H. Matsuki, K. Nagano, and Y. Fujimoto, "Bilateral drive gear—a highly backdrivable reduction gearbox for robotic actuators," *IEEE/ASME Transactions on Mechatronics*, vol. 24, no. 6, pp. 2661–2673, 2019.

[29] T. Yada, "Review of gear efficiency equation and force treatment," *Jsme International Journal Series C-mechanical Systems Machine Elements and Manufacturing*, vol. 40, pp. 1–8, 1997. [Online]. Available: https://api.semanticscholar.org/CorpusID:109798859

[30] N. Zou, Y. Wei, S. Chang, and D. Zhou, "Single planetary mechanism teeth matching conditions," in *Proceedings of the 2015 International Conference on Advanced Manufacturing and Industrial Application*. Atlantis Press, 2015/12, pp. 42–45. [Online]. Available: https://doi.org/10.2991/icamia-15.2015.10

[31] G. M. Maitra, *Handbook of Gear Design*. New Delhi: Tata McGraw-Hill Education Pvt. Ltd., 2010.

[32] W. Roozing and G. Roozing, "Experimental comparison of pinwheel and non-pinwheel designs of 3d-printed cycloidal gearing for robotics," in *2024 IEEE International Conference on Robotics and Automation (ICRA)*, 2024, pp. 7091–7098.